特輯

일본내 연구동향 (6편중 제1편)

Applications of Cure Monitoring Techniques by Using Fiber Optic Strain Sensors to Autoclave, FW and RTM Molding Methods

Takehito Fukuda*, Tatsuro Kosaka, Katsuhiko Osaka
(Department of Intelligent Materials Engineering, Osaka City Unv.)

ABSTRACT

This paper describes applications of cure monitoring techniques by using embedded fiber optic strain sensors, which are extrinsic Fabry-Perot interferometric (EFPI) and/or fiber Bragg grating (FBG) sensors, to three kinds of molding methods of autoclave, FW and RTM molding methods. In these applications, internal strain of high-temperature curing resin was monitored by EFPI sensors. From these experimental results, it was shown that strain caused by thermal shrink at cooling stage could be measured well. In addition, several specific matters to these molding methods were considered. As for an autoclave molding of unidirectional FRP laminates, it was confirmed that off-axis strain of unidirectional FRP could be monitored by EFPI sensors. As for FW molding using room-temperature (RT) cured resin, it was found that the strain outputs from EFPI sensors represented curing shrinkage as well as thermal strain and the convergence meant finish of cure reaction. It was also shown that this curing shrinkage should be evaluated with consideration on logarithmic change in stiffness of matrix resin. As for a RTM molding, both EFPI and FBG sensors were employed to measure strain. The results showed that FBG sensors have also good potential for strain monitoring at cooling stage, while the non-uniform thermal residual strain of textile affected the FBG spectrum after molding. This study has proven that embedded fiber optic strain sensors have practical ability of cure monitoring of FRP. However, development of automatic installation methods of sensors remains as a problem to be solved for applications to practical products.

1. Introduction

In situ monitoring technique by using in situ sensors is a new approach to improve cost and reliability of fiber reinforced plastics (FRP). During molding process of FRP, in situ sensors are used to monitor cure degree, pressure, temperature, voids, defects and residual stress in real time. Such real-time information in materials during molding is available for control of molding process. An optimized curing cycle of FRP moldings let us reduce total molding time and enhance quality of products. A process of quality assurance can be also simplified by this technique. Several kinds of micro sensors, which are fiber optic sensors, dielectric sensors, piezoelectric sensors etc., have been investigated as

* Corresponding Author (E-mail:takehito@mech.eng.osaka-cu.ac.jp)

in situ sensors for monitoring of FRP moldings [1]. During molding process of FRP, these sensors are mainly applied to monitoring of cure process. However, some sensors can be also used in pre-cure process such as injection process of resin [2].

Fiber optic sensors are promised due to their small size, light weight, high strength and high flexibility for cure and health monitoring of FRP. Several kinds of fiber optic sensors, near-infrared spectroscopy (NIRS)-based sensors, fluorimetry-based sensors, refractive index-based sensors and strain/temperature sensors have been proposed for cure monitoring. NIRS-based sensors [3,4] and fluorimetry-based sensors [5,6] can monitor chemical state of resin. Refractive index-based sensors [4,7] can measure refractive index of resin. Embedded fiber optic temperature sensors measure local temperature in composites during cure [8-10]. Measurement of residual strain, which is caused by cure and thermal shrink, can be conducted by embedded fiber optic strain sensors [11-16]. Although most fiber optic sensors for cure monitoring are not available for health monitoring, fiber optic strain sensors have availability both in molding process and in operation.

Several kinds of fiber optic strain/temperature sensors, which are interferometric sensors, extrinsic Fabry-Perot interferometric (EFPI) sensors, fiber Bragg grating (FBG) sensors, Brillouin optical time domain reflectometric (B-OTDR) sensors, etc., can be used for strain measurement. Among these sensors, FBG sensors and EFPI sensors are popular for in situ strain monitoring of FRP molding process due to high accuracy. Several applications of fiber optic strain sensors to cure monitoring have been reported [11-17]. However, more application examples are required to apply this technique to many kinds of FRP molding methods. In this paper, both EFPI and FBG strain sensors were applied to cure monitoring of three molding methods, which are autoclave, FW and RTM molding methods. Then, we made comparative discussions on these experimental results.

2. Fiber optic strain sensors

Fig. 1(a) shows construction of EFPI sensors. EFPI sensor is constructed from two optical fibers, which are fixed with a capillary tube and have half mirrors at the ends of the fibers. The two mirrors compose a Fabry-Perot interferometer. There are two kinds of measurement systems for EFPI sensors. One uses a narrow-band light and another uses a broadband light. The former is a cheaper and suited for a high-speed system, but the system depends on optical power loss. On the other hand, the latter system is independent on optical power loss due to capability of absolute measurement of the cavity length [18]. Then, it is called absolute EFPI (AEFPI). Because applied pressure to FRP vary in molding process, AEFPI is desirable for cure monitoring. In this paper, the latter system was employed for strain acquisition. In that system, the cavity length d was obtained by measuring $\Delta\kappa$, which is a period of the transfer function of the reflected spectrum in wavenumber domain. When the peak positions were obtained from the spectrum as shown in Fig. 1(a), the cavity length can be calculated from λ_1 and λ_N by the following equation.

$$d = \frac{1}{2\Delta\kappa} = \frac{(N-1)}{2}\frac{\lambda_1\lambda_N}{\lambda_N - \lambda_1} \tag{1}$$

Then, the strain output of EFPI sensor can be represented as;

$$\varepsilon_3 = \frac{\Delta d - d_0\alpha_S\Delta T}{L_G} \tag{2}$$

where, L_G is a gauge length, d_0 is an initial cavity length and Δd is a variation of the cavity length.

Fig. 1(b) illustrates construction of FBG sensors and the sensing mechanism. An FBG sensor has a fiber grating, which is a longitudinal periodic variation of refractive index in core of a single mode fiber [19]. When a broadband light is incident into the grating, a narrowband light is reflected. The center wavelength, which is called Bragg wavelength λ_G, shifts when the fiber is stretched. Since the wavelength shift has a linear relationship with variation of the grating period, FBG sensors have capability of absolute measurement of the axial strain. Bragg shift $\Delta\lambda$, which is obtained by subtracting initial Bragg wavelength λ_0 from λ_G, has the following relationship with strain ε_3 and temperature shift ΔT.

$$\frac{\Delta\lambda}{\lambda_0}=\left[1-\frac{n_0^2}{2}\{p_{12}-\nu_s(p_{11}+p_{12})\}\right]\varepsilon_3 + \left(\alpha_s+\frac{1}{n_0}\frac{dn_0}{dT}\right)\Delta T \quad (3)$$

Here, p_{11} and p_{12} are Pockels constants, α_s is coefficient of thermal expansion (CTE), ν_s is Poisson ratio, n_0 is refractive index at $\Delta T=0$. All values belong to FBG sensors.

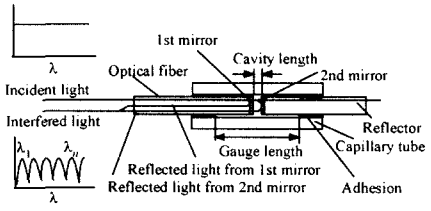

(a) EFPI sensor.

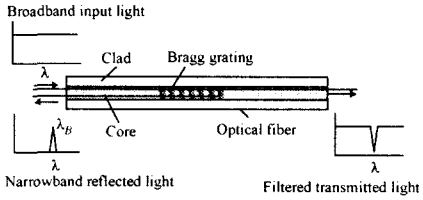

(b) FBG sensor.

Fig. 1 EFPI and FBG strain sensors.

Table 1 shows comparison between properties of EFPI and FBG sensors. EFPI sensors always have larger diameter than FBG sensors. Sensing part of FBG sensors can be easily multiplexed in single fiber, however it is difficult for EFPI sensors. Temperature dependency on strain value is very important for cure monitoring because temperature variation in molding process is usually large. Most of commercial EFPI strain sensors have low thermal sensitivity because the gage length is about 20 times as long as the cavity length. On the other hand, the temperature dependency of FBG sensors is about hundred times as large as EFPI sensors. The last considered properties are effect of strain concentration. It has been reported that strain concentration affect behavior of FBG sensors [20,21]. Then, FBG sensor outputs may be affected by non-uniform strain distribution when they are embedded in loose textile FRP.

Three different fiber optic sensors and three different strain acquisition systems were employed for strain measurements. The FBG sensors have 10 mm gauge length and two kinds of the EFPI sensors have gauge lengths of 4 mm (FEPI-A) and 1 mm (EFPI-B), respectively. These sensors use common optical fibers for communication except their sensing parts. The EFPI sensors have polyimide coating and FBG sensors have UV epoxy coating. The temperature sensitivity of the EFPI-A and the EFPI-B sensors are less than 0.01×10^{-6}/°C.

Table 1 Comparisons of properties between EFPI and FBGsensors

Sensor type	EFPI	FBG
Diameter	Larger diameter (over 200μm)	125μm for commercials
Multiplexing	Difficult	Easy
Strength	Lower	Higher
Resolution	Higher	Lower
Temperature dependency	Lower ($<0.01\times10^{-6}$/°C)	Higher (1.0×10^{-6}/°C)
Strain concentration effect	No	Yes

On the other hand, the following relation among the wavelength shift, ε_3 and ΔT was experimentally obtained.

$$\Delta\lambda=(0.7326\times\varepsilon_3+6.928\times10^{-6}\times\Delta T)\lambda_0 \quad (4)$$

This relation shows that the dependency on temperature is too large to be neglected.

Figure 2 illustrates three kinds of strain acquisition systems used in this study. The acquisition system A consists of an optical spectrum analyzer (OSA), a broadband laser (super luminescence diode; SLD) and a circulator. The acquisition systems B and C use commercial systems of the FBG-IS (Fiber Bragg Grating Interrogation System, Micron Optics, Inc.) and the FTI-Bus 500 (Fiso Technology, Inc.), respectively. The FBG-IS is specialized for measurement of Bragg wavelength from the FBG sensors, and the FTI-Bus, for the EFPI-B sensors. The acquisition system A has lower sensitivity for strain measurement than the acquisition systems B and C. However, the system is useful to obtain extra information except strain because reflected spectrum shape

includes information of disturbance occurring in embedding and ingress/egress sections of fiber optic sensors. In the acquisition system A, measured spectra were sent to PC, then strain was calculated by using the equations (1) and (2) for EFPI sensors or the equation (4) for FBG sensors.

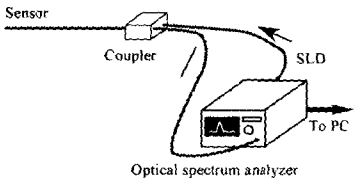

(a) System A; using OSA and SLD

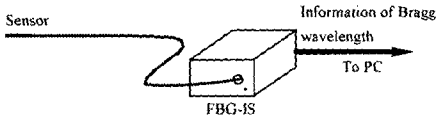

(b) System B; FBG-IS (Micron Optics, Inc., Only for FBG sensors)

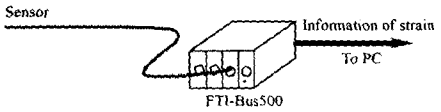

(c) System C; FTI-Bus 500
(Fiso Technology, Inc., Only for EFPI-B sensors)

Fig. 2 Strain acquisition systems for fiber optic sensors.

3. Application to autoclave molding process

3.1 Experimental setup

Internal strain of unidirectional glass GFRP laminates was monitored during autoclave molding process. Twenty plies of glass/epoxy prepreg sheet (GEI300-TX24235 manufactured by Shin-Nippon Chemical Co.Ltd) were used for manufacturing of the laminates. After stacking of ten plies, fiber optic sensors were put on them. Then remaining plies were stacked. In this experiments, EFPI-B sensors and the acquisition system C were used for strain measurement. As shown in Fig. 3, three EFPI sensors were embedded at the angles? of 0°, 45° and 90° from the reinforcing direction. The prepreg lay-up assembly for the autoclave molding is shown in Fig. 4. The patterns of the molding temperature and pressure are shown in Fig. 5. The autoclave chamber used in this experiment is manufactured by Ashida Industrial Co.Ltd. Optical fibers were drawn from the chamber through a hole prepared for the purpose.

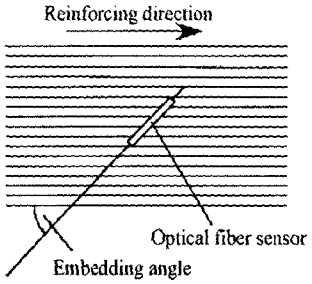

Fig. 3 Embedding angle of EFPI sensors embedded in the laminate.

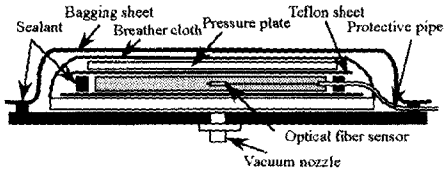

Fig. 4 Prepreg lay-up assembly for the autoclave molding.

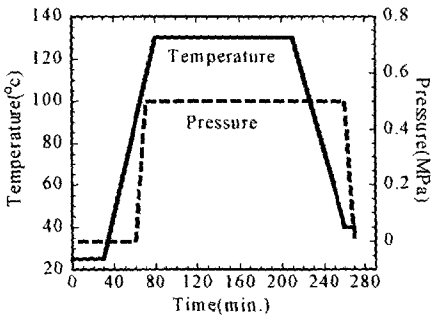

Fig. 5 Molding temperature and pressure in the autoclave molding.

3.2 Results and discussions

The measured internal strains during the autoclave molding are shown in Fig. 6. In the figure, the abscissa and the ordinate designate the strain outputs from the EFPI-B sensors and the molding time, respectively. The measured strain was

almost zero until the molding temperature begins to decrease (point A in Fig. 6). Then, the compressive strain increases with the decreasing temperature at the cooling stage.

From the figure, the sensors output different values after cooling due to orthotropic CTE of the FRP laminate. In order to investigate the strain variation during the cooling stage in detail, the magnified view of Fig. 6(a) at the cooling stage was shown in Fig. 6(b). The figure shows that the strain designates almost the same compressive value for 210-230 minutes. This is unusual behavior because optical fiber sensors were constraint by cured FRP at the cooling stage. The possible reason is an effect of constraint by a pressure plate.

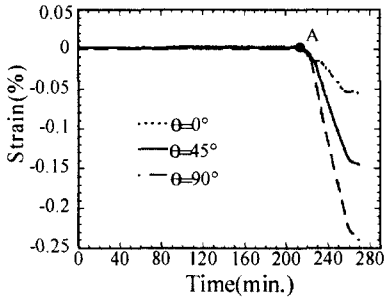

(a) Full time

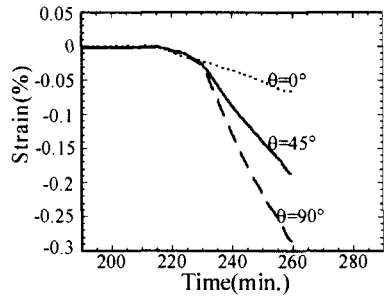

(b) Magnified view at cooling stage

Fig. 6 Internal strain of GFRP laminates during the autoclave molding.

4. Application to filament winding molding process

4.1 Experimental setup

Internal strain measurements of GFRP FW pipes were conducted during cure. The E-glass fiber strands (Nippon Sheet Glass, Co. Ltd.) and the two kinds of matrix resins were used. The vinyl ester (RIPOXY R-802, Showa High Polymer, Co. Ltd.) was cured at the room temperature (RT) and the epoxy resin (EPIKOTE 807, Yuka Shell Epoxy, Co. Ltd.) was cured at the high temperatures (for 2 hours at 100° C and then for 4 hours at 175°C). The strain monitoring system used the EFPI-B sensors and the acquisition system C.

FW pipes were fabricated by the winding machine (Maruto Testing Machine Company). The winding method was a helical winding at 45°. The glass fiber strands, which were impregnated by resin, were wound on a steel mandrel pipe of 30 mm diameter. The strain monitoring system was calibrated to zero strain before the embedding. When the thickness of the pipe reached to the half of the final product, the winding was stopped and the sensor was embedded toward the length of the FW pipe. The reel-type jig was made to rewind the EFPI sensor in the winding process. After the winding process, a thermocouple and a dielectric sensor were attached on the surface of the FW pipe and then the EFPI sensor was connected to the strain measurement system shown in Fig. 7. The total time of the winding was about 40-50 minutes.

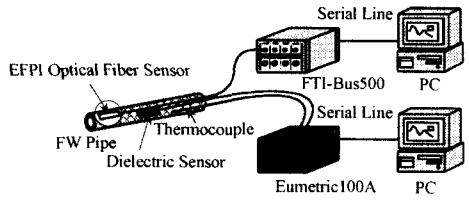

Fig. 7 Experimental setup for cure monitoring of FW pipes.

4.2 Experimental Results and discussions

Fig. 8 illustrates behaviors of the internal strain and temperature of the GF/RIPOXY FW pipe and the RIPOXY resin. The cure monitoring of GF/RIPOXY pipe were conducted for 20 hours at 27 °C (FW1 in Fig. 8) or for 30 hours at 31 °C (FW2 in Fig.8). The cure condition of the RIPOXY resin was the same as the experiment of FW1. The strain output of the sensors embedded in the resin showed zero strain for the first 4-5 hours even though the cure reaction of the resin already started. Thus, it was appeared

that the fiber optic sensor was not constrained by the resin at the early stage of the measurement. On the other hand, the results of the FW pipe showed non-zero strains. This fact implies that the sensor outputs were affected by the reinforcing fiber strands due to the winding force before constraint of the sensors. However, this poor reproducible strain output at the unconstrained stage is not important for strain measurement.

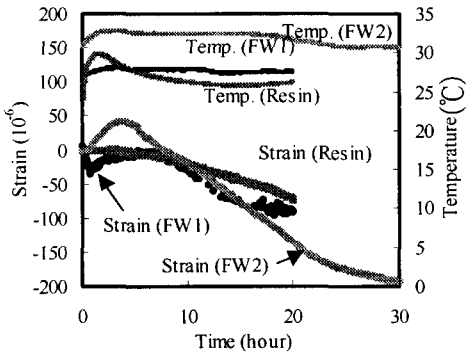

Fig. 8 Internal strain from EFPI sensor and surface temperature of GF/RIPOXY FW pipe (FW1 and FW2) and RIPOXY resin in the RT curing process.

After about 4-5 hours, the strain of the FW pipe and resin decreased until the end of the measurement. It indicates that the bonding between the EFPI sensor and the resin became so strong to constrain the sensor. At the constrained stage, the temperature was almost constant. Then, it was found that the compressive strain was mainly generated by the curing shrinkage though the decrease of the strain includes both the thermal and curing shrinkages. There was a little difference of the strain behavior between FW1 and FW2 after 15 hours because the curing temperatures are slightly different. At the end of the measurement, the strain was not converged for both FW1 and FW2. This represents that the cure did not finish at the end of the measurement. Although the total strain measured in this experiments was very small, it was found that the EFPI-B sensors have enough sensitivity to monitor the curing strain of RT curing resin. Here, we should note that stable condition of temperature is required to measure the curing shrink precisely.

Fig. 9 shows the experimental results of the internal strain and temperature of the GF/Epoxy pipe and the epoxy resin. At the first heating stage, little change in strain was detected before the start of cure at 35 min. Then, it was found that the sensor was not constrained before the curing stage. Temperature of FW pipe was lower than that of resin because the reaction heat increased temperature of the resin in the cup. After the sensor was constrained by the resin, the sensor measured the tensile strain due to the thermal expansion of the resin. Then, the compressive strain by the curing shrinkage was observed at the second isothermal stage.

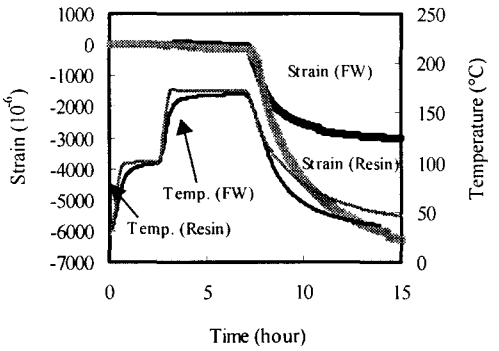

Fig. 9 Internal strain from EFPI sensor and surface temperature of GF/Epoxy FW pipe and Epoxy resin in the high-temperature curing process.

At the end of this stage, the strain value was almost converged. Figure 10 illustrates the strain behavior of the GF/Epoxy pipe as a function of temperature. It can be obviously seen that the strain-temperature curve has three stages, which are thermal expansion, curing shrinkage and thermal shrinkage. Here, it should be noted that both of the thermal expansion and the curing shrinkage are included into the strain value in the curing stage. In this experiment, the

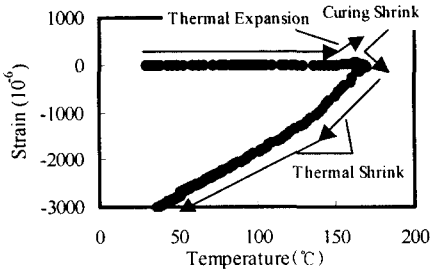

Fig. 10 Strain behavior of GF/Epoxy FW pipe as a function of temperature.

residual strain by the curing shrinkage was almost zero due to the cancellation of the tensile strain by the thermal expansion. At the cooling stage, only the thermal shrink strain was observed because the curing shrink was converged.

4.3 Evaluation of curing shrink by using FEA

From the cross-sectional observation of the molded FW pipe, it was found that the resin rich region around the embedded EFPI sensor was formed after the cure. Then, the effect of the resin rich region on the strain output should be studied. In addition, it is well known that stiffness of a thermosetting resin changes on a logarithmic scale in curing process. Then, the effect of the stiffness changes of the matrix resins on the sensor outputs should be considered. In this paper, finite element analyses (FEA) of the FW pipes with an embedded EFPI sensor were conducted with the following assumptions.

(i) There is no sliding on the interfaces.
(ii) Poisson's ratio of resin is constant.
(iii) FW pipe is axisymmetric 45° angle-ply laminate
(iv) Temperature is constant

A part of the FW pipe with the embedded EFPI sensor was modeled for the FEA as shown in Fig. 11. The model was constructed from the GFRP part, the resin part and the EFPI sensor part. The material properties of the GFRP were calculated from that of the fiber strand and the matrix resin with the measured volume fraction V_f, which is 0.44 for the GF/RIPOXY and 0.42 for the GF/Epoxy. E_1 and ν_{12} were calculated by the rule of mixture and the other constants were from Uemura's method [22]. Shape and dimension of the resin part were decided from the cross-sectional observation. Since curing shrink has an analogical effect with a thermal shrink, the thermal load was used for the FEA instead of the curing shrinkage of the resin. Then, the effect of the curing shrinkage was calculated with setting the CTE of glass to zero. The FEA was conducted by using the linear static analysis solver of MSC NASTRAN for Windows (MSC Corp.).

Since it is considered that E_m changes from MPa range to GPa range after the sensor is constrained in the curing process, the FEA were conducted in the range of E_m from 0.005 GPa to the values of the cured resins. The numerical results of the GF/RIPOXY and the GF/Epoxy FW pipes are shown in Fig. 12. Here, the ordinate is the strain transmission coefficient $\eta = \varepsilon_z^{EFPI}/\varepsilon_z^{GFRP}$, where ε_z^{EFPI} is the axial strain of the EFPI sensor and ε_z^{GFRP} is that of the GFRP part as shown in Fig. 11. The abscissa is E_m on logarithmic scale. To investigate the effect of the resin rich region, the FEA without the resin part were also conducted. The numerical results without the resin part are also plotted in Fig. 12.

From the figure, it is found that the results of the GF/RIPOXY and the GF/Epoxy are almost the same. This implies that h is not so sensitive to the change in Poisson's ratio of the resin. The numerical results show that h changes sensitively when $E_m < 0.5$ GPa. For the effect of the resin

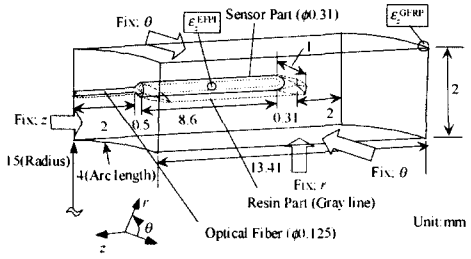

Fig. 11 Schematic view of part model of FW pipe with embedded EFPI sensor for FEA.

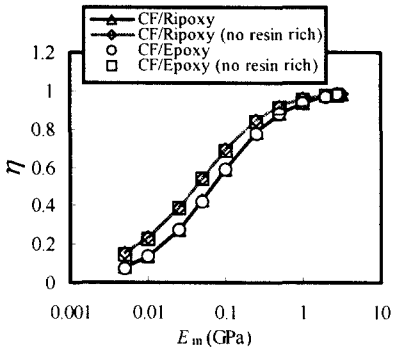

Fig.12 Strain transmission coefficient h of FW GF/RIPOXY and GF/Epoxy pipe as functions of E_m.

rich region, it strongly affects h in the range of $E_m < 1.0$ GPa. Since it is considered that $E_m \ll 1.0$ GPa at the initial stage of the cure, it is concluded that the effect of the stiffness change and the resin rich region on the monitoring of the curing shrinkage cannot be ignored. Therefore, the curing shrinkage should be estimated with including the effects for the RT curing process. On the other hand, it can be considered that E_m of the epoxy is small until the second heating stage for the high temperature curing process due to the high speed of the reaction. At the second heating stage, the curing shrink is canceled out by the thermal expansion. Thus, the effects may be negligible at the second isothermal stage of the high temperature curing process.

5. Application to RTM molding process

5.1 Experimental setup

Internal strain measurements of textile GFRP during RTM molding process were conducted. Two different molds were used for manufacturing of FRP. Schematic views of mold A and B are illustrated in Fig. 13 (a) and (b), respectively. The FBG sensors, the EFPI-A sensors and the acquisition system A were used in the mold A. In the mold B, the acquisition system B was used for the EFPI-B sensors, and the acquisition system C, for the FBG sensors. Fiber optic sensors, thermocouples and dielectric sensors were embedded in the center layer of preforms before resin injection process. Embedding angles of fiber optic sensors were 90° in the mold A and 0° in the mold B from resin flow direction. Optical fibers were fixed to one fabric preform by stitching it. The mold A has a slide to draw optical fibers from the mold. In the mold B, optical fibers were drawn from the surface of specimen and the egress hole of the upper plate was sealed by a plastic plug.

The epoxy resin (EPIKOTE 807, Yuka Shell Epoxy, Co. Ltd.) was injected into the mold by applying pressure to a resin tank. After finish of the resin injection, optical fiber sensors were connected to the strain acquisition systems and a dielectric sensor, to dielectric measurement system. The internal temperature was measured by an embedded thermocouple. The specimens were cured for 2 hours at 100° C and for 4 hours at 175°C in a furnace. Strain from the FBG sensors was compensated by using temperature measured by the embedded thermocouple. After the end of the cure reaction, the molds were cooled to room temperature naturally.

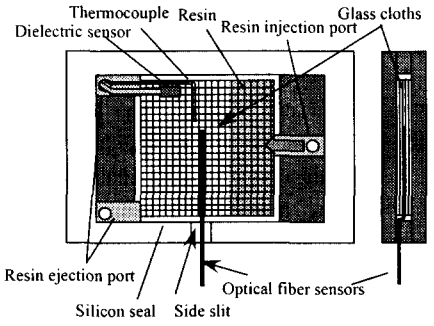

(a) Mold A

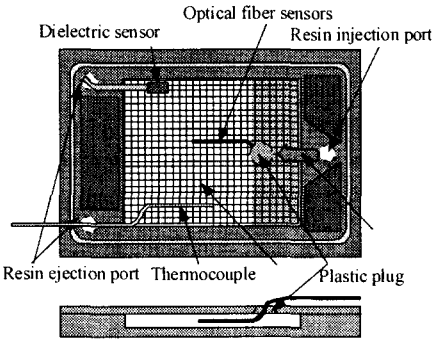

(b) Mold A

Fig. 13 Schematic views of RTM molding systems.

5.2 Results and discussions

Fig. 14 shows the typical relationship between temperature and log ion viscosity measured in the mold A. From the results, the molding process is considered to consist of five stages, which were the first heating stage (I), the first isothermal stage (II), the second heating stage (III), the second isothermal stage (IV) and cooling stage (V). The cure reaction of the resin started after the mixture of the resin with the cure agent and proceeded slowly at the resin injection process. Since it took a few hours to fill the mold with the resin, the ion viscosity was already high at the beginning of the measurement as shown in Fig. 14. The ion

viscosity decreased at the stage I and then increased at the beginning of the stage II. This indicates that speed of the cure reaction became faster beyond 100 °C. The convergence of the ion viscosity indicates finish of the cure reaction at the end of the stage IV.

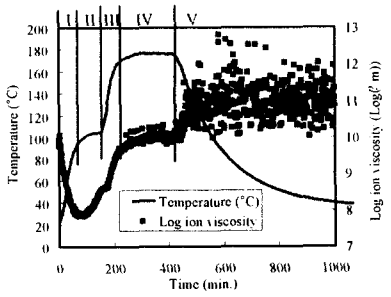

Fig. 14 Typical relationship between temperature and log ion viscosity.

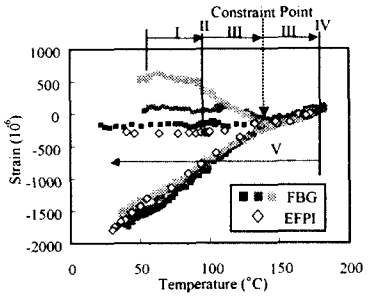

Fig. 15 Strain-temperature relationships obtained from the FBG and the EFPI-A sensors in the mold A.

Fig. 15 shows strain-temperature relationships obtained from the FBG and the EFPI-A sensors in the mold A. It is noted that baselines of the strain-temperature curves were shifted so that the curves matched to zero strain at 175°C. The knee points of the strain-temperature curves can be seen at the middle of the stage III. It appeared that the sensors were constrained by the reacting resin after this knee point because the sensors began to indicate tensile strain by heating. Then, the knee point was named constraint point. From the figure, it was found that the strain-temperature curves from the FBG sensors had poor reproducibility before constraint of the sensors at the stage III. From the constraint point to the stage IV, the strain increased linearly with the temperature change. At the stage V, the strain decreased linearly with the temperature decreasing. It can be seen that the FBG sensors have good reproducibility at the stage V. In addition, the results of the EFPI-A showed good agreement with those of the FBG sensors in range of 175-80°C at the cooling stage. Therefore, it can be concluded that the FBG and the EFPI-A sensors are reliable at cooling stage of curing process of RTM moldings.

Fig. 16 shows strain-temperature relationships obtained from the FBG and the EFPI-B sensors in the mold B. From the figure, it is obvious that strain resolutions of the acquisition systems B and C are better than the acquisition system A Unlike the mold A, the results of the mold B represented good reproducibility during molding in the mold B. Therefore, it can be concluded that the embedding configuration parallel to resin flow is better for reproducible strain measurement by the FBG sensors. As for EFPI sensors, it was found that strain behavior of the EFPI-B sensors is completely different form the EFPI-A. It can be considered that this difference occurred by difference of gauge length. Gauge length of the EFPI-B, is almost half of reinforcing period of FRP. Then, it is thought that the EFPI-B sensors were affected by local strain distribution near fiber strand. Therefore, it can be concluded that the gauge length of embedding sensor is important parameter to measure precise strain in loose textile FRP.

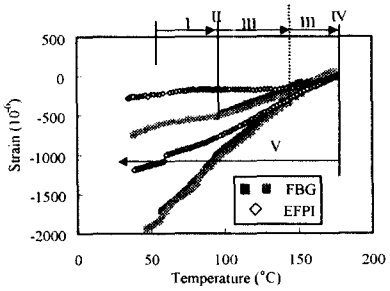

Fig. 16 Strain-temperature relationships obtained from the FBG and the EFPI-B sensors in the mold B.

Observations of reflected spectra from the FBG sensors were conducted using the acquisition system A. Figure 17 shows reflected spectra from the embedded FBG sensors at cooling stage. From the figure, it was found that the reflected spectra were deteriorated after the cooling. This deterioration caused the reduction of the optical power and precision of the strain measurement. The spectrum shape was changed

gradually with decrease of temperature. Then, it can be concluded that non-uniform residual stress distribution caused by loose textile preforms deteriorated the spectrum. Stress analysis around the embedded sensor is necessary for more quantitative discussions.

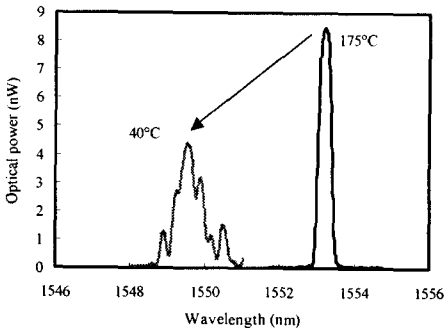

Fig. 17 Reflected spectra from the FBG sensor in the mold A.

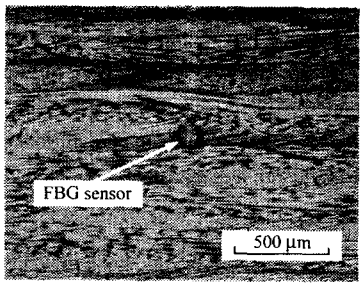

(a) Around the embedded FBG sensor

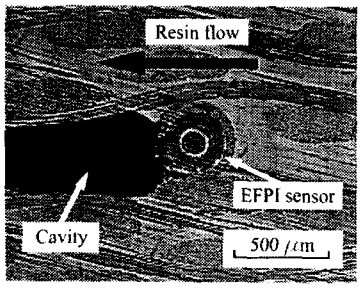

(b) Around the embedded EFPI sensor

Fig. 18 Cross-sectional photographs of FRP molded by the mold A (optical fibers were embedded transversely against resin flow direction).

After the experiments, the specimens were cut across the embedded optical fibers. Then the cross sections were observed by an optical microscope. Figures 18(a) and (b) show the cross-sectional photographs of the specimens molded by the mold A, where the FBG and the EFPI-A sensors were embedded, respectively. Figure 18(a) shows that the embedding condition of FBG sensor was good. On the other hands, a large void was observed near the EFPI-A sensor as shown in Fig. 18(b). It was obvious that this void was formed due to the high viscous resin and the large diameter of the EFPI-A sensor. Low viscous resin is necessary for the use of the EFPI-A sensors since formation of the dry spot depends on the viscosity of resin as well as diameter of fiber optic sensors. When fiber optic sensors were embedded along resin flow direction, large voids could not be observed. Therefore, it can be concluded that FBG sensors are more suitable than EFPI sensors for RTM molding when the embedding angle is large.

6. Conclusions

Cure monitoring techniques by using embedded EFPI and/or FBG fiber optic strain sensors were applied to three kinds of molding methods, which are autoclave, FW and RTM molding methods. From the experimental results, it was found that strain caused by thermal shrink at cooling stage of high-temperature curing resin could be measured with good precision by EFPI sensors. Then, it can be concluded that the residual strain caused by large and complex-shape FRP can be monitored despite molding methods. In addition to the above experiments, several specific matters to these molding methods were considered.

As for autoclave molding methods, it was confirmed that off-axis strain of unidirectional FRP could be monitored by EFPI sensors. As for RT curing process of FW pipe, it was found that the strain outputs from EFPI sensors represented curing shrinkage of resin and the convergence meant finish of cure reaction. It was also shown that this curing shrinkage should be evaluated with consideration on logarithmical change in stiffness of matrix resin. As for RTM molding methods, both EFPI and FBG sensors were employed to measure strain. The results showed that FBG sensors have also good potential for strain monitoring at cooling stage,

while the thermal residual strain of textile FRP, which was not uniform after cooling down to room temperature, affected FBG spectrum.

This study has proven that strain monitoring of FRP curing process by using embedded EFPI and FBG fiber optic strain sensors can be applied practically to FRP molding methods. However, manual installations of sensors were conducted and the inefficiency will be a problem to be solved for practical applications. Therefore, automatic installation methods of sensors should be developed for practical use in future.

Acknowledgement

This work was performed under the management of Research and Development Institute of Metals and Composites for Future Industries (RIMCOF) and New Energy and Industrial Technology Development Organization (NEDO). And it is a part of R&D Projects of Smart Materials and Structural Systems.

References

1) T. Fukuda and T. Kosaka, "Smart Monitoring Techniques for Composites Molding Processes," *Materials Science Research International- Special Technical Publication*, Vol. 2, 2001, pp. 51-57.
2) S. Motogi, T. Itoh, T. Fukuda, K. Yamagishi, S. Kitade and H. Morita, "Development of Multi-Functional Sensor for Resin Transfer Molding," *12th International Conference on Composite Materials (ICCM-12), Paris, France*, Pap1260.pdf (PDF file), 1999.
3) G.R. Powerll, P.A. Crosby, D.N. Waters, C.M. France, R.C. Spooncer and G.F. Fernando, "In-Situ Cure Monitoring Using Optical Fibre Sensors - A Comparative Study," *Smart Materials and Structures*, Vol. 7, 1998, pp. 557-568.
4) P.A. Crosby, G.R. Powerll, G.F. Fernando, C.M. France, R.C. Spooncer and D.N. Waters, "In Situ Cure Monitoring of Epoxy Resins Using Optical Fibre Sensors," *Smart Materials and Structures*, Vol. 5, 1996, pp. 415-428.
5) H.J. Paik and N.H. Sung, "Fiberoptic Intrinsic Fluorescence for In-Situ Cure Monitoring of Amine Cured Epoxy and Composites," *Polymer Engineering and Science*, Vol. 34, No. 12, 1994, pp. 1025-1032.
6) D.L. Woerdenman and R.S. Parnas, "Plastics Analysis: Cure Monitoring in RTM Using Fluorescence," *Plastics Engineering*, Vol. 51, No. 10, 1995, pp. 25-27.
7) Y.M Liu, C. Ganesh, J.P.H. Steele and J.E. Jones, "Fiber optic sensor development for real-time in-situ epoxy cure monitoring," *Journal of Composite Materials*, Vol. 31, No. 1, 1997, pp. 87-102.
8) L. Lai, G. Carman, S.Chiou, P. Kukuchek and D. Echternach, "Processing monitoring of carbon/phenolic composites using smart sensors," *Smart Materials and Structures*, Vol. 4, 1995, pp. 118-125.
9) R.C. Foedinger, D.L. Rea, J.S. Sirkis, C.S. Baldwin and J.R. Troll, "Embedded Fiber Optic Sensor Arrays for Structural Health Monitoring of Filament Wound Composite Pressure Vessels," *Proc SPIE*, 3670, 1999, pp. 289-301.
10) P.A. Crosby, C.Doyle, C. Tuck, M. Singh and G.F. Fernando, "Multi-Functional Fiber Optic Sensors for Cure and Temperature Monitoring," *Proc SPIE*, 3670, 1999, pp. 144-152.
11) T. Kosaka, K. Osaka, M. Sando, and T. Fukuda, "Curing Strain Monitoring of FRP FW Pipe with EFPI Fiberoptic Sensors," *Materials Science Research International- Special Technical Publication*, Vol.2, 2001, pp. 100-104.
12) K. Osaka, T. Kosaka, Y. Asano and T. Fukuda, "Off-axis Strain Monitoring of FRP Laminates in Autoclave Molding," *Materials Science Research International-Special Technical Publication*, Vol.2, 2001,. pp. 105-109.
13) T. Kosaka, K. Osaka, Y. Asano and T. Fukuda, "Cure Monitoring of FRP by FBG Fiberoptic Sensors in RTM Molding Process," *Proc. of the 13th International Conference on Composite Materials (ICCM-13)*, pcd1611 (PDF), 2001.
14) T. Kosaka, H. Kurimoto, K. Osaka, A. Nakai, T. Osada, H. Hamada and T. Fukuda, "Development of Smart Braided Composites by Using Fiberoptic Strain Sensors," *Proc. of the 7th Japan International SAMPE Symposium*, 2001, pp. 99-102.
15) A.L. Kalamkarov, S.B. Fitzgerald, D.O. MacDonald, "The Use of Fabry Perot Fiber Optic Sensors to Monitor Residual Strains during Pultrusion of FRP Composites," *Composites: Part B*, Vol. 30, 1999, pp. 167-175.
16) H,K, Kamg, D.H. Hang, C.S. Hong and C.G. Kim, "Cure Monitoring of Composite Laminates Using Fiber Optic Sensors," *Proceedings of The 2nd Korea-Japan Joint Symposium on Composite Materials, Seoul, Korea*, 2001,

pp. 179-184.

17) V.M. Murukeshan, P.Y. Chan, L.S. Ong, L.K. Seah, "Cure Monitoring of Smart Composites Using Fiber Bragg Grating Based Embedded Sensors," *Sensors and Actuators: A*, Vol. 79, 2000, pp. 153-161.

18) C. Belleville and G. Duplain, "White-Light Interferometric Multimode Fiber-Optic Strain Sensor;" *Optic Letters*, Vol. 18, 1993, pp. 78-80.

19) Y.J. Rao, "Recent Progress in Applications of In-Fibre Bragg Grating Sensors;" *Optics and Lasers in Engineering*, Vol. 31, 1999, pp. 297-324.

20) K.J. Peters, M. Studere, J. Botsis, A. Iocco, H.G. Limberger and R.P. Salathe, "Measurement of Stress Concentrations Using Embedded Optical Fiber Bragg Grating Sensors," *Proc. SPIE*, 3670, 1999, pp. 195-206.

21) Y. Okabe, S. Yashiro, T. Kosaka, and N. Takeda, "Detection of Transverse Cracks in CFRP Composites Using Embedded Fiber Bragg Grating Sensors," *Smart Materials and Structures*, Vol. 9, No. 6, 2000, pp. 832-838.

22) M. Uemura and N. Yamada, "Elastic Constants of Carbon Fiber Reinforced Plastic Materials, *Journal of the Society of Materials Science," Japan*, 24(257), 1975, pp. 156-163, (in Japanese).